1.3 ON THE EFFECTS OF HE-DPA INTERACTIONS ON CAVITY EVOLUTION IN TEMPERED MARTENSITIC STEELS UNDER DUAL ION IRRADIATION—

Takuya Yamamoto, Yuan Wu, G. Robert Odette (University of California Santa Barbara), Kiyohiro Yabuuchi, Sosuke Kondo, Akihiko Kimura (Kyoto University)

OBJECTIVE

The objective of this research is to characterize cavity evolution in irradiated 9Cr tempered martensitic steels (TMS) and how this is affected by the starting microstructure and irradiation variables.

SUMMARY

We filled some gaps in our cavity evolution database on normalized and tempered 9Cr martensitic steels (TMS) F82H under Fe^{3+} plus He^{+} dual ion beam irradiation (DII) at 500°C. New experiments were conducted at ≈ 30 appm He/dpa at relatively low nominal damage rate of 6.5×10^{-4} dpa/s. The cavity evolution database at 500°C now includes 321 material-dpa-He-dpa rate DII conditions. Two distinct trends of higher and lower swelling rates versus dpa are observed. Here we compare the detailed evolution of the cavity size distributions with increasing dpa and He to seek clues about the reasons for these differences in behavior. The higher swelling rate case was generally associated with higher dpa rates, fewer cavities and stronger bi-modality, compared to the lower swelling rate case.

BACKGROUND

As reported previously [1-6], we have been carrying out systematic 500°C DII studies in the DuET facility at Kyoto University (Japan) at various nominal He/dpa ratios and dpa rates, that are nominally defined at the depth of 600 nm. Here we update the DII database and report an analyses of cavity evolution (and swelling) trends in TMS F82H Mod.3 (F82HM3) for a very wide range of DII dpa, He and He/dpa.

PROGRESS AND STATUS

Experimental Procedure

Details of alloys and DII experiments can be found in [4]. Table 1 summarizes nominal He and dpa irradiation conditions at two reference depths in F82HM3 analyzed in this report at a reference depth of ≈ 600 nm. The irradiations targeted two *nominal* dpa, three He/dpa ratios and two dpa rate conditions. However, taking advantage of the varying spatial distributions of dpa, He and He/dpa, we actually characterized the microstructures over a much wider range irradiation conditions. The latest DII experiment aimed at achieving high dpa and He/dpa at a relatively low dpa rate, filling a major hole in our database at 500°C. Through focus series bright field TEM was used to characterize the cavities (bubbles and voids) in a series of 100 nm slices from near the surface to beyond the end of the range of the 6.4 MeV Fe^{3+} ions. The location specific cavity volume fractions were used to analyze void swelling trends as a function of dpa and He/dpa ratio. The dpa are based on SRIM calculations using the Kinchin-Pease model, with Fe displacement energy of 40 eV [7,8]. We analyzed size distribution evolution at two He/dpa ratio conditions (≈ 30 and 50 appm/dpa) with an emphasis on studing the He bubble to void transition.

Results

Cavity evolution trends

Here cavity evolution trends as a function of dpa and He/dpa are quantified in terms of the bubble and void volume fraction, f, and size (diameter, d) distributions. Earlier analyses showed that variations in the average void diameter, $\langle d_v \rangle$, and number density, N_v, are less sensitive to local microstructure variations than f; and that the total $f \approx f_v$. We separate voids from bubbles by assuming a (≈ critical) threshold diameter of 4 nm for the latter. This threshold is not fixed or rigorous, but corresponds to a dip that is

often observed between the two bubble and void peaks in the cavity size distribution. We have also previously noted that there are two distinct groups showing higher and lower swelling rates. Figure 1 summarize these two trends including the new data that falls in the low swelling group. The larger swelling rates, that was also identified in F82H IEA [1] (not included in this report), are commonly observed only at the highest nominal dpa rate of 1.3 - 1.5 x 10^{-3} dpa/s. However, there is one case in F82HM3 at the high dpa rate that showed a low swelling rate trend. Since the F82H IEA with a higher swelrate and the one F82HM3 showing a lower swelling rate were DII side-by-side, the differences are not due to an unexpectedly high temperature or large variations in dpa and He/dpa. Thus the varied swelling rates are more likely due to starting microstructural differences between the two F82H heats.

Table 1. Irradiation conditions analyzed in this report

T (^{o}C)	Nominal Condition (@550-650nm)				Peak He (@1000-1100nm)		
	dpa	He (appm)	He/dpa	dpa/s	dpa	He (appm)	He/dpa
500	26	1210	47	5.0 x 10^{-4}	45	2100	47
500	9.9	457	46	5.2 x 10^{-4}	17	795	46
500	10	480	47	5.1 x 10^{-4}	18	840	47
500	26	390	15	5.1 x 10^{-4}	44	670	15
500	30	848	29	1.5 x 10^{-3}	51	1467	29
500	30	1200	47	1.3 x 10^{-3}	45	2100	47
500	45	1290	28	8 x 10^{-4}	79	2230	28
500	51	1360	27	8.6 x 10^{-4}	88	2350	27
500	52	2327	45	6.5 x 10^{-4}	89	4024	45

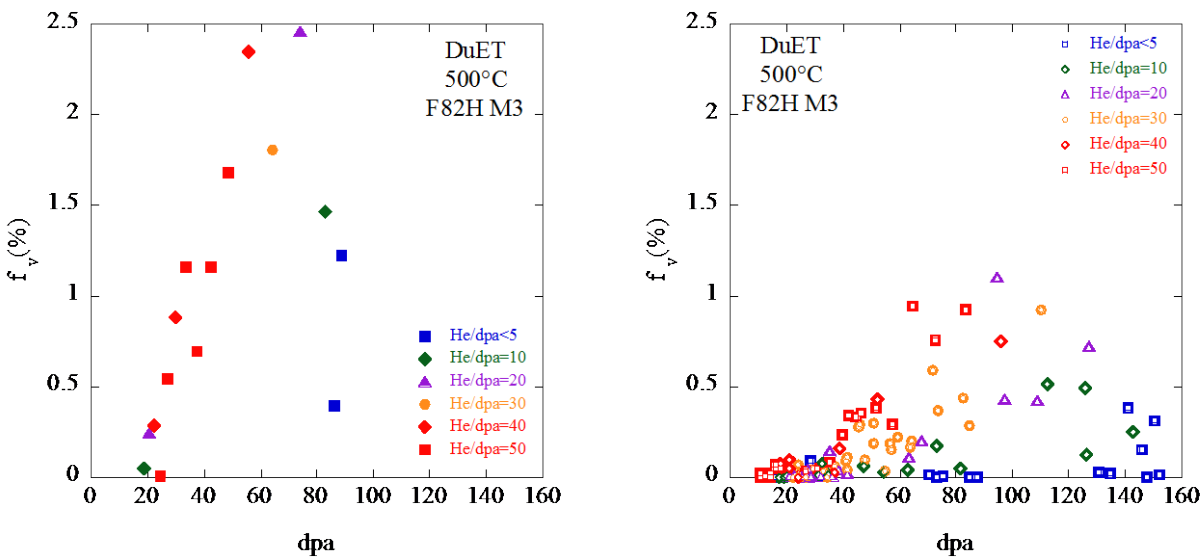

Figure 1 Void volume fraction – dpa trends at various He/dpa ratios in DII F82HM3 in two data groups respectively showing swelling rates that are: a) higher, and, b) low swelling.

Figure 2 shows size distribution evolution for (a) high and (b) low swelling groups at a He/dpa ratio of ≈ 50 ± 5 appm/dpa. The lack of fully systematic trends in individual cases reflects large specimen point-to-point variations in the cavity number densities, which are, in turn, likely mostly due to local starting microstructural variations. The number shown by the histograms are the dpa and He (appm) based on SRIM calculations. The third number in parenthesis is the amount of He estimated to be in the cavities; this will be discussed in a future report. The dashed line at 4 nm is what we assumed to be the nominal

critical size for stably growing bubbles by He additions, to convert to unstably growing voids. The low swelling case in Figure 2a shows a mostly unimodal size distribution, but at higher dpa and He, the distribution gradually blends into the void category of cavities. In contrast, for the higher dpa rate case shown in Figure 2b, the cavity distributions are more bimodal, or the bubbles are almost fully transformed to voids, even relatively low dpa and He. There are also far fewer bubbles and voids in this case. That is, fewer cavities reach critical size sooner, since He is partitioned to a smaller number of bubbles that thus individually contain more He.

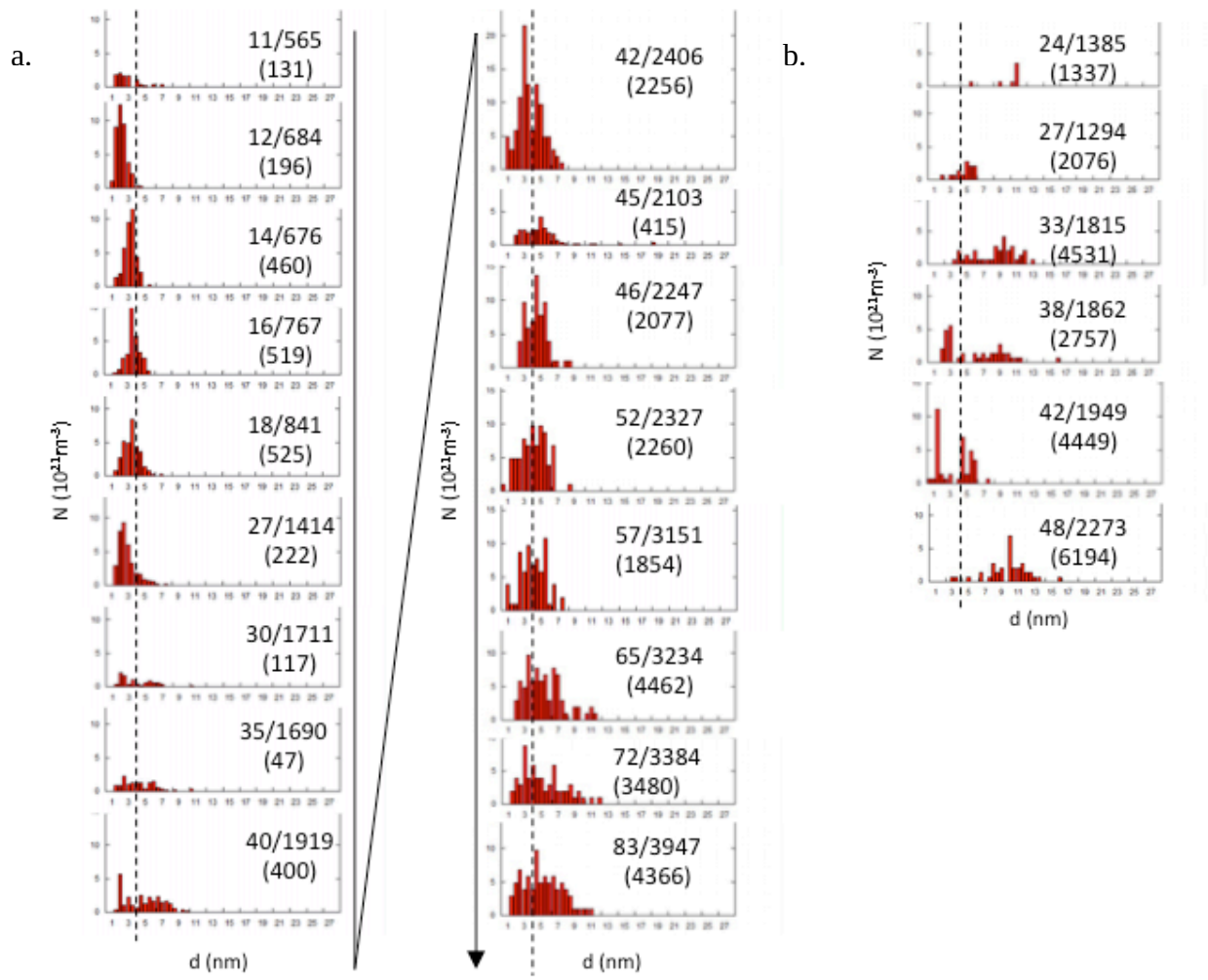

Figure 2. The cavity size distribution evolution in DII F82HM3 at ≈ 50±5 appm He/dpa for: a) a lower nominal dpa rate of ≈ 6 x 10^{-4} dpa/s (left two columns); and, b) for a higher nominal dpa rate of ≈ 1.5 x 10^{3} dpa/s.

Figure 3 shows the cavity size distribution evolutions for irradiations at 30±5 apmm He/dpa. The series of plots in Figure 3a, at low nominal dpa rates, are similar to, but somewhat more bimodal than, those in Figure 2a. The bimodal pinch-off size appears to be much smaller than 4 nm in this case. The series of size distributions in Figure 3b at high nominal dpa rates resulted in low swelling because of the small number of voids and large number of bubbles. However the distinct bimodality is consistent with the nominal d_c = 4 nm critical diameter. Notably by 64 dpa, shown in Figure 3c, all the smaller number of cavities are voids.

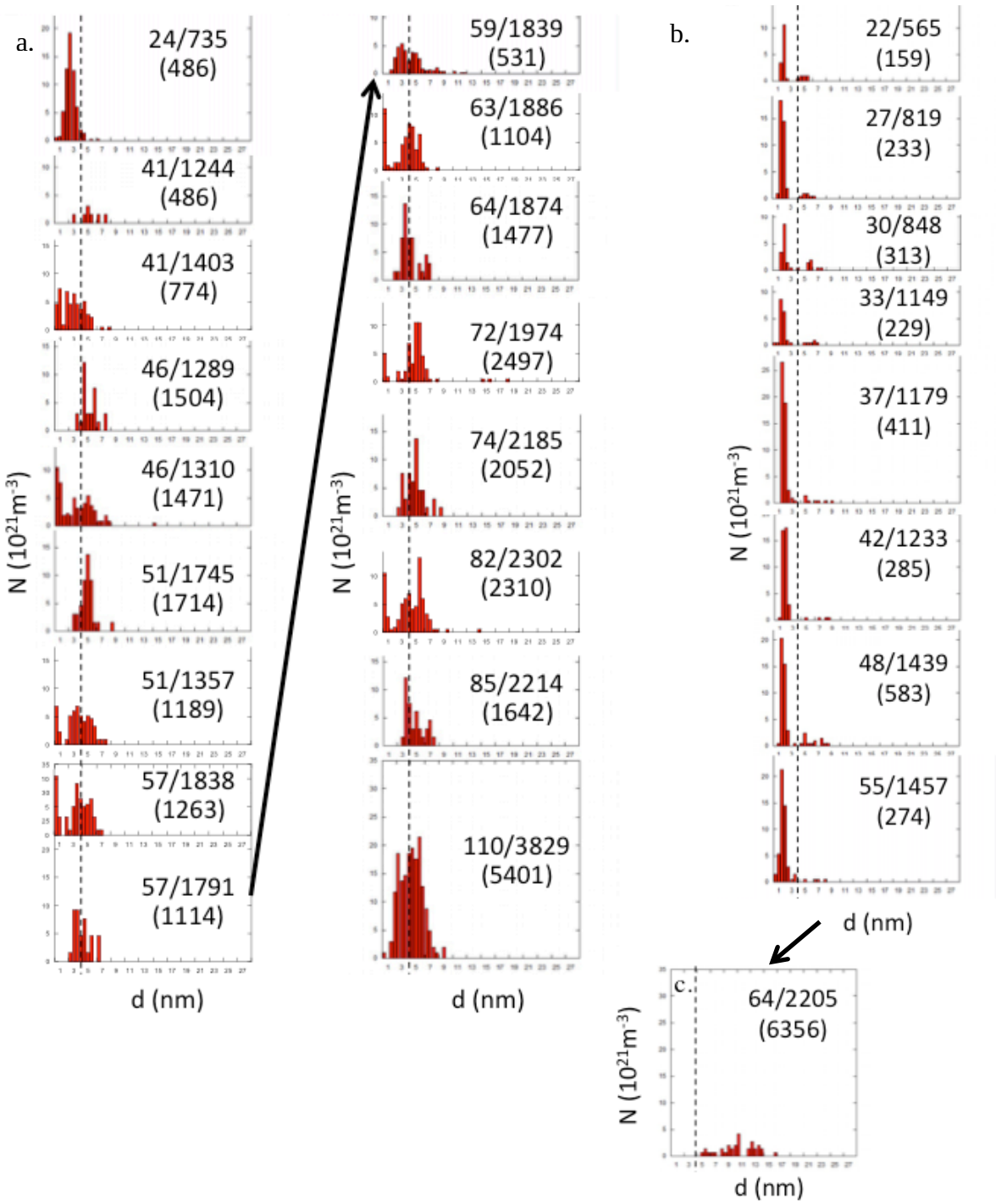

Figure 3. Size distribution evolution in DII F82HM3 at ≈ 30±5 appm He/dpa: a) at low nominal dpa rate of ≈ 6.8 x 10^{-4} dpa/s (left two columns) compared with b) high ≈ 1.5 x 10^{-3} dpa/s nominal rate to up to 55 dpa and c) to 64 dpa.

Discussion and Summary

This work in progress will be discussed in more detail in future reports and publications. In summary: a) a nominal critical size d_c = 4 nm is generally consistent to the observed cavity size distribution evolution trends; b) there is lower swelling at low dpa rates and the cavity size distributions are more unimodal; c) swelling is higher and cavity size distributions are more bimodal at high dpa rates; and, d) swelling is lower at higher dpa rates even with distinct bimodality, when more numerous bubbles may retard the bubble-to-void transition.

Acknowledgements

The dual ion-beam irradiations were conducted under the support of the "Joint Research Program on Zero-Emission Energy Research, Institute of Advanced Energy, Kyoto University (ZE28A-03, 27A-22, 26A-16, 25A-19, 24A-13 and 23B-3). The work performed at UCSB was supported by the U. S. Department of Energy, Office of Fusion Energy Sciences, under Contract DE-FG03-94ER54275. We acknowledge the contributions of the NSF sponsored UCSB Microstructure and Microanalysis Facility. We are also grateful for generous support of research materials, F82H mod.3 from Dr. K. Shiba, (JAEA, Japan).

References

[1] T. Yamamoto, Y. Wu, G.R. Odette, K. Yabuuchi, S. Kondo, A. Kimura, *Fusion Materials Semiannual Report 6/30/2015* DOE/ER-313/58 (2015) 12

[2] G.R. Odette, T. Yamamoto, Y. Wu, S. Kondo, A. Kimura, *Fusion Materials Semiannual Report 12/31/2014* DOE/ER-313/57 (2015) 8

[3] T. Yamamoto, Y. Wu, G.R. Odette, S. Kondo, A. Kimura, *Fusion Materials Semiannual Report 6/30/2014* DOE/ER-313/56 (2014) 194

[4] T. Yamamoto, Y.Wu, G.R. Odette, K. Yabuuchi, S. Kondo, A. Kimura, J. Nucl. Mater. 449 (2014) 190

[5] T. Yamamoto, Y.Wu, G.R. Odette, S. Kondo, A. Kimura, *Fusion Materials Semiannual Report 6/30/2013* DOE/ER-313/54 (2013) 6.

[6] T. Yamamoto, Y. Wu, G.R. Odette, K. Yabuchi, A. Kimura, *Fusion Materials Semiannual Report 12/31/2010* DOE/ER-313/49 (2011) 1.

[7] ASTM E521-96 (2009), ASTM

[8] R.E. Stoller, M.B. Toloczko, G.S. Was, A.G. Certain, S. Dwaraknath, F.A. Garner, Nuc Instr Mehtods Phys Res B 310 (2013) 75.